Research Article   **Open Access**

Flood Susceptibility Appraisal in Ponnaiyar River Basin, India using Frequency Ratio (FR) and Shannon's Entropy (SE) Models

Jothibasu A. and Anbazhagan S.

Centre for Geoinformatics and Planetary Studies, Department of Geology, Periyar University, Salem, India

Abstract In any Watershed management studies, demarcation of flood prone area is one of the key tasks. Flood management is essential to shrink the flood effects on human lives and livelihoods. Main goal of the present research is to investigate the application of the Frequency Ratio (FR) and Shannon's Entropy (SE) models for flood susceptibility appraisal of Ponnaiyar River basin in Tamil Nadu, India. Initially, the flood inventory map was prepared using overlay analysis (slope, 20 meter contour intervals and drainage patterns) and extensive field surveys. In total, 136 flood locations were noted in the study area. Out of these, 95 (70%) floods were randomly selected as training data and the remaining 41 (30%) floods were used for the validation purposes. Further, flood conditioning factors such as lithology, land-use, distance from rivers, soil depth, rainfall, slope angle, slope aspect, curvature, topographic wetness index (TWI) and altitude were prepared from the spatial database. Then, the receiver operating characteristic (ROC) curves were drawn for produced flood susceptibility maps and the area under the curves (AUCs) was computed. The final results indicated that the FR (AUC = 80.20%) and SE (AUC = 79.30%) models have almost similar and reasonable results. Therefore, these flood susceptibility maps can be useful for researchers and planner in flood mitigation strategies.

Keywords *Geographic Information System; Remote Sensing; Flood Susceptibility; Ponnaiyar River*

1. Introduction

Flood is one of the most common natural disaster events and it creates many environmental problems due to rapid urban growth and climate change (Kjeldsen, 2010). A deep tropical depression came through the Bay of Bengal and hit the south-eastern coast of India on 10-11 November 2015, causing heavy rain. Heavy rain resumed during Nov 16-19, with 30-37 cm of rain accumulating over the 9-day period. After pausing for several days, heavy rains have resumed in early December and in some locations rain is projected to continue until 8-10 December. Chennai received over 33 cm of rain in a 24-hour period from December 1-2, causing widespread flooding and damage. In Tamil Nadu, Chennai city, Cuddalore, Kanchipuram, and Tiruvallur districts are worst affected. Reports are estimating 347 people have lost their lives in Tamil Nadu which can be more. The floods which occurred are the worst in 100 years and the people got stranded in the midnight since flood water entered into the houses while they are asleep, especially in Chennai. The Government of India has

declared Chennai a National Disaster zone, and National Disaster Response Force carried out rescue operations in the city (JNA, 2015). It is motivated to demarcate flood prone area in the study area. Early warnings and emergency responses to floods are needed, so that governments and agencies can prevent as much damage as possible (Feng and Wang, 2011). In natural hazards research, enormous databases are habitually needed (Regmi et al., 2013). These are not easy to collect, and in some cases a lack of appropriate data can hamper research (Liu and De Smedt, 2004). Natural factors such as hydrological and meteorological characteristics, soil types, geological structures, geomorphology, and vegetation are the most influential contributors to flooding. Human interference in natural cycles by cutting trees and building with impervious materials can accelerate flooding.

From sustainable development point of view, the flood hazard management is very essential for future (Feng & Wang, 2011; Esteves, 2013; Schober et al., 2015). However, negative consequences of flood can be applied by integrated approaches to flood hazard management (Anbazhagan and Dash, 2003; Masood & Takeuchi, 2012; Jourde et al., 2014). Remote sensing techniques coupling with GIS tools can provide a good platform to combine, manipulate and analyses the information for the determination of potential hazard areas very quickly and more efficiently (Saha et al., 2005; Pradhan et al., 2011; Devkota et al., 2013; Wang et al., 2013; Pourghasemi et al., 2014). The most popular methods in natural hazard modeling are ANN (Pradhan and Buchroithner, 2010; Pradhan et al., 2010b), analytic hierarchy process (AHP) (Yalcin, 2008), frequency ratio (FR) (Pradhan et al., 2011), logistic regression (LR) (Pradhan, 2010a,b) and fuzzy logic (Pradhan, 2011). Shafapour Tehrany et al. (2013) compared the prediction performances of two different methods such as rule-based decision tree and combination of FR and logistic regression statistical models for flood susceptibility mapping at Kelantan, Malaysia. Their result demonstrated that the area under the curve (AUC) for decision tree and the ensemble FR and LR models was 87 and 90%, respectively. Lee et al. (2012a) applied FR model for flood susceptibility mapping in Busan, South Korea. The results showed that FR model is very efficient for flood susceptibility modeling. Shannon's entropy is the average unpredictability in a random variable, which is equivalent to its information content. The entropy of flood refers to the extent that the various controlling flood occurrences influence the flood susceptibility. Several influencing factors give extra entropy into the index system. Therefore, the entropy value can be used to calculate objective weights of the index system (Jaafari et al., 2014). The main objective of the present research was to assess and compare flood susceptibility maps produced using two statistical GIS-based approaches, i.e. FR and SE models in the Ponnaiyar river basin, Tamil Nadu, India.

2. Study Area

Ponnaiyar River basin an interstate river is one of the largest rivers of the state of Tamil Nadu, often reverently called 'Little Ganga of the South'. The river has supported may a civilizations of peninsular India across the history and continues to play a vital role in supplying precious water for drinking, irrigation and industry to the people of the states of Karnataka, Tamil Nadu and Pondicherry. The study area extends over approximately of 11,595 sq.km, and lies between 11˚35' and 12˚35' N latitudes and 77˚45' and 79˚55' E longitudes (Figure 1). Ponnaiyar River originates on the south eastern slopes of Chennakesava Hills, northwest of Nandidurg of Kolar district in Karnataka State at an altitude of 1000m above mean sea level (amsl). The total length of Ponnaiyar River is 432km of which 85km lies in Karnataka state, 187km in Dharmapuri, Krishnagiri and Salem districts, 54km in Thiruvannamalai and Vellore districts and 106km in Cuddalore and Villupuram districts of Tamil Nadu. The Cuddalore and Villupuram districts are the most affected flood area in the river basin. The first spell witnessed intensive flooding in Cuddalore where most of the water bodies were full and the associated breaching affected the communities' life damaging houses and infrastructure etc., (Figure 2). The Ponnaiyar basin is predominantly built up with granite and gneisses rocks of Archean period. The fifteen years (2000-2014) average annual rainfall in the basin is 969 mm. The climate in general is hot; April and May being the hottest months of the year when the temperature rises to 34˚C.
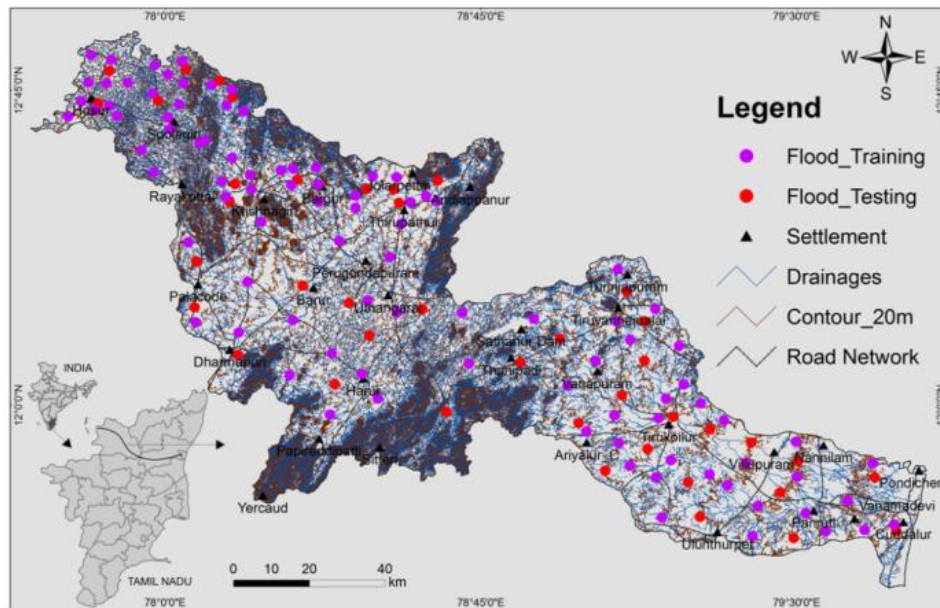
Figure 1: Study area and flood locations of Ponnaiyar river basin

Figure 2: Photographs shows the severity of the flood that occurred in 2015

3. Data Used and Methodology

3.1. Identify Flood Locations

A basin level flood-prone area map provides the regional level planners and decision makers with information useful in formulating broad policies to guide the future development of flood plains. In the context, the flood-prone map was prepared using SRTM satellite data were applied to create a digital elevation model (DEM) of the study area with spatial resolution of 90 m. The slope and contour maps were prepared using DEM. Which include contour lines with 20 m interval connecting points on the ground surface that have the same elevation showing the configuration and elevation of the land

surface. The areas subject to flooding were delineated from readily available information for quick appraisal rather than by detailed field surveys.

3.2. Flood Conditioning Factors

In order to execute flood susceptibility mapping it is necessary to find out the flood conditioning factors (Kia et al., 2012). Therefore, a flood related spatial database should be created. Through the knowledge gathered from the literature review and field investigation the conditioning factors were chosen (Smith and Ward, 1998). Hence, ten flood conditioning factors such as lithology, land use / land cover (LULC), soil depth, distance from main river, rainfall, altitude, curvature, slope, topographic wetness index (TWI) and aspect were selected for the susceptibility analysis and the spatial database of these factors was compiled. The lithology is considered as one of the most important indicators of hydro-geological features which play a fundamental role in both the porosity and permeability of aquifer materials (Ayazi et al., 2010; Charon, 1974). The analog lithology map (1:100,000) was obtained from the Geological Survey of India (GSI, 1998) and the digital lithology map was generated using ArcGIS 9.3 (Figure 3a). According to Geological Survey of India the lithology of the study area is varied and covered by twenty two rock types.

Land use types play a significant role, which directly or indirectly influence on some of hydrological processes components such as infiltration, evapotranspiration and run-off generation. Land use types within the study area are agriculture land, built-up land, forest cover, river, water body, barren land, and grass land (Figure 3b). Built-up areas, which are mostly made by impervious surfaces, increase the storm run-off and inundation (Shafapour Tehrany et al., 2013). On the other hand, agricultural areas are less prone to flooding due to the positive relationship between infiltration capability and vegetation density. The land use / land cover map was prepared from IRS P6 LISS III image through supervised classification using maximum likelihood algorithm, and false color composite (FCC) techniques in ENVI 4.3 software.

Distance from main rivers play significant roles in hydro-geological systems. It is one of the main conditioning factors due to its impact on the flood magnitude (Glenn et al., 2012). It is controls the stability of a slope is the saturation degree of the material on the slope. The closeness of the slope to drainage structures is another important factor in terms of stability. Streams may adversely affect stability by eroding the slopes or by saturating the lower part of material until resulting in water level increases (Gokceoglu and Aksoy, 1996). The distance from river map was produced using the buffer tool in ArcGIS 9.3 and was classified into five classes (Figure 3c). Soil is a complex biogeochemical material on which plants may grow. Information on the type of soil is often needed as a basic input in hydrologic evaluation. Mapping soil usually involves delineating soil types that have identifiable characteristics. The delineation is based on many factors garment to soil science such as geomorphologic origin and conditions under which the soil formed (Vieux, 2004). Soil depth is one of the most important factors in the surface and subsurface runoff generation and infiltration process (Mogaji et al., 2014). The soil depth map was obtained from the Central Groundwater Board (CGWB, 2012). There are four classes of soil depth in the study area (Figure 3d).

The monsoon flooding takes place after heavy rain, so this factor should be considered as one of the main contributors in flood occurrence (Bajabaa et al., 2013). The monthly records of rainfall amount for thirty rain-gauge stations within the study area for a period of 15 years (2000–2014) were obtained from the Tamil Nadu State Surface and Groundwater Division database. The resulting map was classified into five major classes: 688-850, 850-923, 923-987, 987-1046 and 1046-1195 mm/year (Figure 3e). Average annual rainfall in the study area varies in the range of 688 mm to 1195 mm. North eastern and south western part receive high rainfall (>987mm) whereas southeastern and northwestern part receive low rainfall (<923mm).

The slope map of the study area was generated based on DEM using the Spatial Analysis tools in ArcGIS 9.3. Based on the quantile classification scheme (Tehrany et al., 2014), the slope angle map was grouped into six classes such as <7˚, 7˚-15˚, 15˚-20˚, 20˚-25˚, 25˚-30˚ and >30˚ (Figure 3f). Aspect is related to the main precipitation direction and the physiographic trends (Ercanoglu and Gokceoglu, 2002). Slope aspect layer was extracted from DEM and divided into nine classes including ten directions and flat based on normal or common standard classification (Figure 3g). Curvature, (Tc) was calculated from the DEM (Figure 3h). The map comprises five classes ranging from very high class to very low class. Negative values for curvature (<−2) correspond concave and accumulation zones, zero values for curvature represent the flat and transitional zones and the positive values for curvature represent the convex and dissipation zones (Florinsky, 2000).

Topographic Wetness Index (TWI) has been widely used to explain the impact of topography conditions on the location and size of saturated source zones of surface runoff generation. It is defined as (Moore et al., 1991):

$$TWI = In\left(\frac{A_s}{tan\beta}\right) \quad (1)$$

Where, A_S is the cumulative upslope area draining through a point (per unit contour length) and β is the slope gradient (in degree)

In this study, TWI map is grouped into four classes using quantile classification scheme (Tehrany et al., 2014) (Figure 3i). The tendency of water to accumulate at any point in the catchment (in terms of α) and the tendency of gravitational forces to move that water down slope (indicated in terms of tan b as an approximate hydraulic gradient) are considered by the ln β tanα index. Primarily, the water infiltration depends upon material properties such as permeability and pours water pressure on the soil strength.

Different altitudes have altered climate conditions, and this caused differences in soil condition and vegetation type (Aniya, 1985). Altitude map of the study area was created from the DEM. The altitude map was grouped into six classes: -4 to 205 m, 205–386 m, 386-556 m, 556–750 m, 750–1009 m, and 1009-1635 m based on the quantile classification method (Figure 3j) (Tehrany et al., 2013).

3.3 Frequency Ratio (FR) Model

Frequency ratio (FR) model is a bivariate statistical approach which can be used as a useful geospatial assessment tool to determine the probabilistic relationship between dependent and independent variables, including multi-classified maps (Oh et al., 2011). Recently, FR model has been successfully used for flood susceptibility mapping by Tehrany et al. (2014a), Rahmati et al. (2015). In fact, the FR is defined as the ratio of the area where flood occurred in the total study area. FR model structure is based on the correlation and observed relationships between each flood conditioning factor and distribution of flood locations. FR value in each class of the groundwater-related factor can be expressed based on Eq. 2:

$$FR = \left(\frac{A/B}{C/D}\right) \quad (2)$$

Where,
A is the number of flood training set for each factor;
B is the number of total flood training set in study area;
C is the number of pixels in the class area of the factor;
D is the number of total pixels in the study area

The complete calculation of weight determination for individual parameters is presented in Table 1. In a given pixel, flood susceptibility index (FSI) can be determined by summation of pixel values according to Eq. (3):

$$FSI = Li_{FR} + LU_{FR} + Dmr_{FR} + Sd_{FR} + Rf_{FR} + Sad_{FR} + Sa_{FR} + Tc_{FR} + TWI_{FR} + At_{FR} \quad (3)$$

3.4. Shannon's Entropy Model

The entropy index is a measure of "evenness" extent to which groups are evenly distributed among organizational units (Massey and Nancy, 1988). In the present study, an attempt has been made to assess flood susceptibility mapping using entropy. More precisely, Theil (1972) defined entropy index as a measure of the average difference between a unit's group proportions and that of the system as a whole. There is a one-to-one relationship between the quantity of entropy of a system and the degree of disorder called Boltzmann principle and has been used to represent the thermodynamic status of a system (Yufeng and Fengxiang, 2009). Shannon improved upon the Boltzmann principle and established an entropy model for information theory. The equations implemented to calculate the information coefficient (V_j) representing the weight value for the parameter as a whole (Bednarik et al., 2010) are given as following (Eqs. 4–8):

$$E_{ij} = \frac{FR}{\sum_{j=1}^{M_j} FR} \quad (4)$$

where, FR is the frequency ratio and E_{ij} is the probability density.

$$H_j = -\sum_{i=j}^{M_j} E_{ij} Log_2 \ E_{ij}, j = 1, \dots, n \quad (5)$$

$$H_{jmax} = log_2 M_j, \quad M_j = number \ of \ classes \quad (6)$$

$$I_j = \left(\frac{H_{jmax} - H_j}{H_{jmax}} \right), I = (0,1), j = 1, \dots_n \quad (7)$$

$$V_j = I_j FR \quad (8)$$

Where, H_j and H_{jmax} are entropy values;
    I_j is the information coefficient and
    M_j is the number of classes
    V_j depicts the resultant weight value for the parameter as a whole
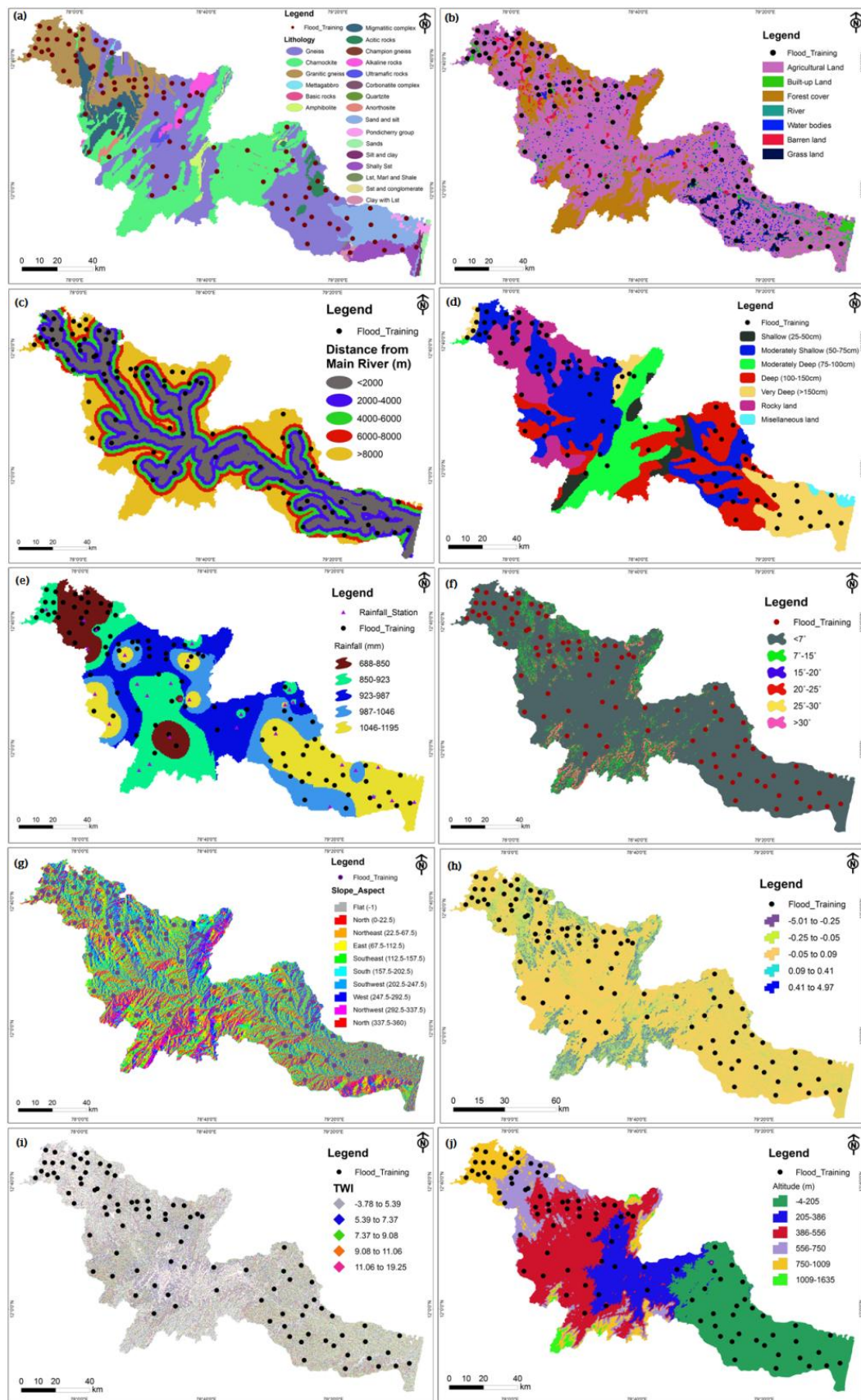
Figure 3: *Flood conditioning factors of Ponnaiyar river basin; (a) lithology altitude (b) land use (c) distance from main river (d) soil depth (e) rainfall (f) slope angle (degree) (g) slope aspect (h) curvature (i) Topographic Wetness Index (TWI) and (j) altitude*

Table 1: Frequency Ratio and Shannon's Entropy values for the considered flood condition factors

Factors	No. of pixel in domain	Percent age of domain	No. of well	Percent age of well	FR	Eij	Hj	Hmax	Ij	Vj	Vj final
Lithology											
Gneiss	11933	34.879	23	24.211	0.69	0.061	1.053	1.342	0.215	0.149	2.435
Charnockite	10057	29.395	29	30.526	1.04	0.092					
Granitic gneiss	4519	13.208	23	24.211	1.83	0.162					
Mettagabbro	25	0.073	0	0.000	0.00	0.000					
Basic rocks	66	0.193	0	0.000	0.00	0.000					
Amphibolite	377	1.102	2	2.105	1.91	0.169					
Migmatitic complex	1777	5.194	4	4.211	0.81	0.072					
Granitic/acidic rocks	663	1.938	2	2.105	1.09	0.096					
Champion gneiss	12	0.035	0	0.000	0.00	0.000					
Alkaline rocks	567	1.657	3	3.158	1.91	0.168					
Ultramafic	165	0.482	0	0.000	0.00	0.000					
Ultrabasic syenite	10	0.029	0	0.000	0.00	0.000					
Quartzite	5	0.015	0	0.000	0.00	0.000					
Anorthosite	153	0.447	0	0.000	0.00	0.000					
Sand and silt	2278	6.658	6	6.316	0.95	0.084					
Pondicherry	202	0.590	0	0.000	0.00	0.000					
Sands	150	0.438	0	0.000	0.00	0.000					
Alter seq. of sand / silt and clay	128	0.374	0	0.000	0.00	0.000					
Shaly sand stone	1001	2.926	3	3.158	1.08	0.095					
Lime stone, marl and shale	14	0.041	0	0.000	0.00	0.000					
Sand stone and conglomerate	7	0.020	0	0.000	0.00	0.000					
Clay with limestone	104	0.304	0	0.000	0.00	0.000					
Land use											
Agricultural land	24296	71.014	81	85.263	1.20	0.189	0.802	0.845	0.050	0.060	0.354
Built-up land	1153	3.370	0	0.000	0.00	0.000					
Forest cover	5859	17.125	6	6.316	0.37	0.058					
River	437	1.277	2	2.105	1.65	0.260					
Water bodies	1260	3.683	0	0.000	0.00	0.000					
Barren land	814	2.379	5	5.263	2.21	0.349					
Grass land	394	1.152	1	1.053	0.91	0.144					
Soil Depth											
Shallow (25-50cm)	1457	4.259	3	3.158	0.74	0.121	0.788	0.845	0.066	0.049	0.467
Moderately shallow (50-75cm)	10091	29.495	28	29.474	1.00	0.162					
Moderately deep (75-100cm)	4831	14.120	18	18.947	1.34	0.218					
Deep (100-150cm)	7802	22.804	12	12.632	0.55	0.090					
Very deep (>150cm)	4932	14.416	18	18.947	1.31	0.214					
Rocky land	4821	14.091	16	16.842	1.20	0.194					
Miscellaneous land	279	0.815	0	0.000	0.00	0.000					
Distance from river (m)											
<2000	9219	26.946	33	34.737	1.29	0.250	0.712	0.778	0.084	0.108	0.504
2000-4000	7253	21.200	15	15.789	0.74	0.144					
4000-6000	5463	15.968	18	18.947	1.19	0.230					
6000-8000	4247	12.413	16	16.842	1.36	0.263					
>8000	8031	23.474	13	13.684	0.58	0.113					
Rainfall (Rf)											
688-850	3947	11.537	10	10.526	0.91	0.184	0.695	0.778	0.105	0.096	0.634

Class											
850-923	7505	21.936	20	21.053	0.96	0.193					
923-987	7937	23.199	22	23.158	1.00	0.201					
987-1046	6420	18.765	19	20.000	1.07	0.215					
1046-115	8404	24.564	24	25.263	1.03	0.207					
Altitude											
(-4-205)	463487	33.577	28	29.474	0.88	0.157	0.747	0.778	0.039	0.034	0.234
205-386	208941	15.136	13	13.684	0.90	0.162					
386-556	399278	28.925	25	26.316	0.91	0.163					
556-750	160107	11.599	14	14.737	1.27	0.227					
750-1009	133540	9.674	15	15.789	1.63	0.292					
1009-1635	15038	1.089	0	0.000	0.00	0.000					
Total Curvature											
(-5.01--0.25)	34153	2.474	2	2.105	0.85	0.182	0.669	0.903	0.259	0.220	2.071
(-0.25--0.05)	275679	19.971	18	18.947	0.95	0.203					
(-0.05-0.09)	947734	68.657	66	69.474	1.01	0.217					
0.09-0.41	102835	7.450	8	8.421	1.13	0.242					
0.41-4.97	19990	1.448	1	1.053	0.73	0.156					
Slope angle (Degree)											
<7˚	1206725	87.419	80	84.211	0.96	0.193	0.698	0.778	0.103	0.099	0.618
7˚-15˚	84829	6.145	11	11.579	1.88	0.378					
15˚-20˚	35695	2.586	2	2.105	0.81	0.163					
20˚-25˚	27425	1.987	1	1.053	0.53	0.106					
25˚-30˚	18224	1.320	1	1.053	0.80	0.160					
>30˚	7493	0.543	0	0.000	0.00	0.000					
Topographic wetness index											
(-3.78-5.39)	95719	6.934	17	17.895	2.58	0.369	0.844	0.845	0.0004	0.001	0.003
5.39-7.37	440145	31.886	31	32.632	1.02	0.146					
7.37-9.08	576050	41.731	21	22.105	0.53	0.076					
9.08-11.06	172320	12.483	16	16.842	1.35	0.193					
11.06-19.25	96157	6.966	10	10.526	1.51	0.216					
Slope aspect											
Flat (-1)	7252	0.525	1.00	1.05	2.00	0.171	1.07	1.146	0.066	0.133	0.930
North (0-22.5)	84014	6.086	11.00	11.58	1.90	0.162					
Northeast (22.5-67.5)	170927	12.383	15.00	15.79	1.28	0.109					
East (67.5-112.5)	210918	15.280	13.00	13.68	0.90	0.076					
Southeast (112.5-157.5)	218733	15.846	12.00	12.63	0.80	0.068					
South (157.5-202.5)	171230	12.404	13.00	13.68	1.10	0.094					
Southwest (202.5-247.5)	146330	10.601	9.00	9.47	0.89	0.076					
West (247.5-292.5)	145311	10.527	9.00	9.47	0.90	0.077					
Northwest (292.5-337.5)	158753	11.501	5.00	5.26	0.46	0.039					
North (337.5-360)	66923	4.848	7.00	7.37	1.52	0.129					

The result ranges between 0 and 1. The closer the value is to the number 1, the greater the imbalance is 0. The complete calculation of weight determination for individual parameters is presented in Table 1. In flood susceptibility mapping, the entropy measures and reflects the spatial association between the conditioning factors and flood occurrences. The flood susceptibility index can be determined by summation according to Eq. (9).

$$FSI = Li_{FR}2.435 + LU_{FR}0.354 + Dmr_{FR}0.504 + Sd_{FR}0.467 + Rf_{FR}0.634 + Sad_{FR}0.618 + Sa_{FR}0.930 + Tc_{FR}2.071 + TWI_{FR}0.003 + At_{FR}0.234 \quad (9)$$

3.5. Validation Method

From scientific significance viewpoint, validation is considered to be the most important process of modeling (Chung and Fabbri, 2003). Therefore, it is very important to evaluate the resultant FSI. The receiver operating characteristics (ROC) curve was applied to determine the accuracy of the FSI. The FSI delineated in the current study was verified using the flood locations in the validation datasets. Based on the flood inventory data, the accuracy assessment of the flood susceptibility mapping was made. In total, 136 flood locations were noted in the study area. Out of these, 95 (70%) floods were randomly selected as training data and the remaining 41 (30%) floods were used for the validation purposes. The ROC curves were then obtained by considering cumulative percentage of probability index maps (on the x axis) and the cumulative percentage of flood occurrence (on the y axis). The area under the curve (AUC) was calculated based on ROC curve analysis and it demonstrates the accuracy of a prediction system by describing the system's ability to expect the correct occurrence or non-occurrence of pre-defined "events" (Jaafari et al., 2014). Finally, using the quantitative and qualitative relationship between the AUC value and prediction accuracy can be grouped as very high, high, moderate, low and very low flood occurrences in the study area. The brief methodology used in the present study area shown in Figure 4.
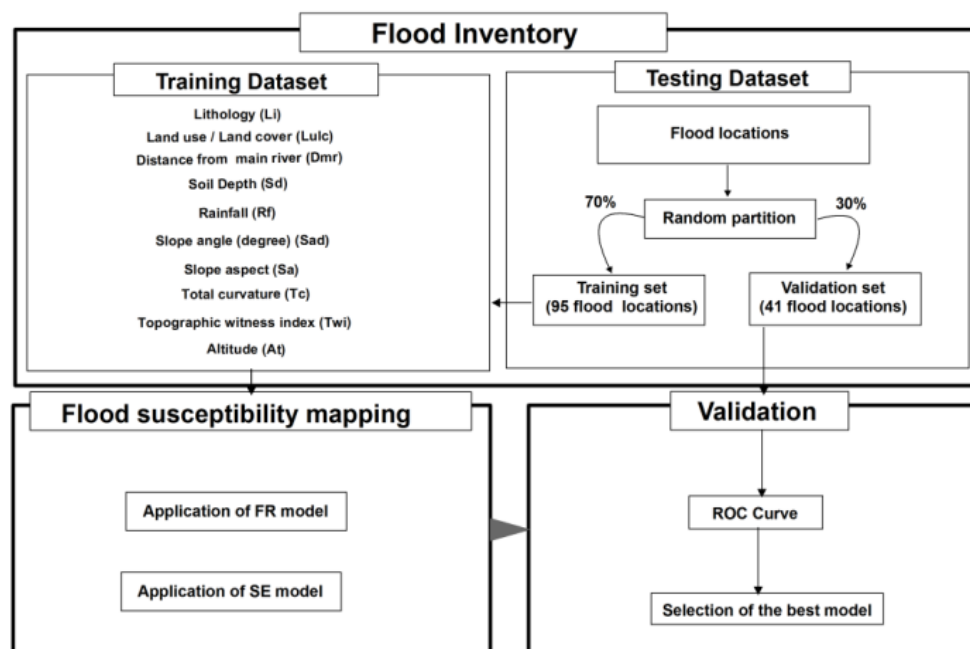

Figure 4: Flowchart showing the methodology adopted in this study

4. Results and Discussion

Frequency Ratio methods were applied to determine the level of relationship between flood locations and conditioning factors. In general, the FR value of 1 indicates an average correlation between flood locations and effective factors (Pradhan, 2010). If the FR value would be larger than 1, there is a high correlation, and a lower correlation equals to the FR value lower than 1 (Lee et al., 2012a). The analysis of FR for the relationship between flood location and lithology units indicates that amphibolites and Alkaline rocks have the highest FR value (1.91) have the most probability for flooding in the study area. The agricultural and barren lands have values of 1.20 and 2.21, respectively, indicating that the probability of flood occurrence in these land-use types is very high. For distance from river in the range 2000–4000 m and >8000 m, there is a low probability of flooding; in contrast, distances in the range <2000 m, 4000–6000 m and 6000–8000 m have the highest values (1.29, 1.19, and 1.36, respectively). These results demonstrated that the flooding mostly occurs near to the river bank and

rarely far from the rivers. The results of soil depth displayed that moderately deep, very deep and rocky land have the highest value of FR (1.34, 1.31 and 1.20 respectively).

The slope angle indicates that class 7°–15° has the highest FR value (1.88), and other indicating a low probability. This means that flood occurrence probability decreases with increasing in slope angle. In the case of slope aspect, flood event is most abundant on flat (FR = 2.00) and northwest-facing slopes (FR = 0.46), have the lowest abundance. Based on the curvature, the (0.09-0.41) shape has the highest FR value (1.13) indicates that the most probability for flooding. That shape retains surface run-off for a longer period especially during heavy rainfall. Therefore, it is more prone for flooding compared to the other shapes. Flood locations are more concentrated in areas with a TWI (-3.78-5.39) (FR = 2.58) and altitude classes of 750-1009 m (FR = 1.63). In the case of altitude, analysis of FR values demonstrated that the flood occurrence cannot occur in the high elevation regions of the study area. Finally, based on Equation (2), the final flood susceptibility map obtained by the FR model is shown in Figure 5.
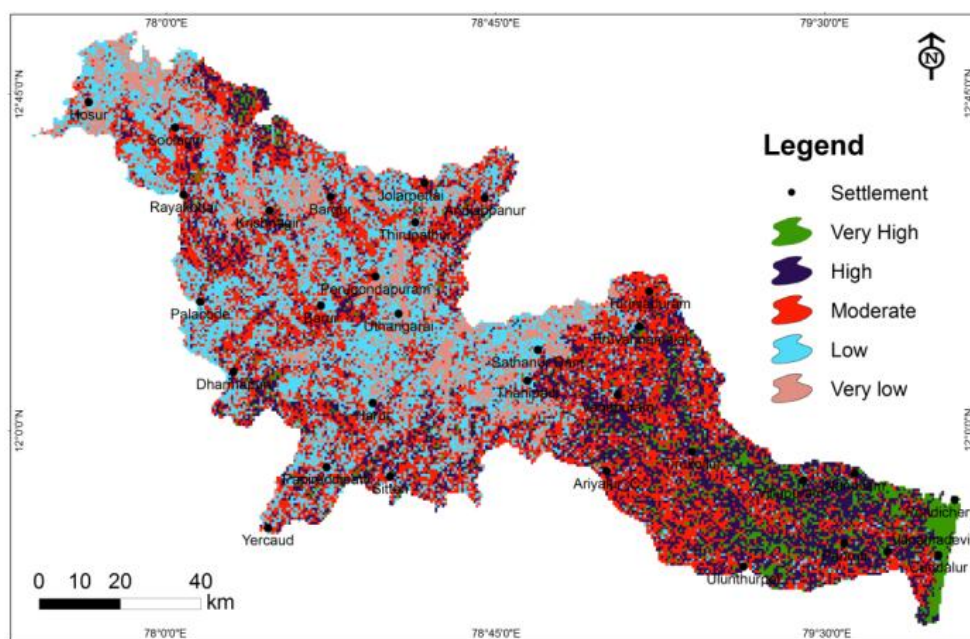

Figure 5: Flood susceptibility map of FR model in Ponnaiyar River basin

In the present study, all parameters of SE model were calculated for each conditioning factor, which is shown in Table 1. Based on the results obtained from the entropy, the lithology and curvature represented highest flood susceptibility in the study area (Vj final, 2.435, 2.071 respectively) showing maximum flood susceptibility. The land-use weights of factors were 0.802, 0.845, 0.050, and 0.060, respectively. The entropy values of distance from the river indicated positive influence in flooding. The analysis of SE for the relationship between flood occurrence and slope angle indicated that positive influences in flooding. In the case of slope aspect and plan curvature, flat area had a strong positive correlation with flood occurrence. Eij values increases by increasing classes of TWI. Moore et al. (1991) stated that TWI represents the effect of topography on the location and size of saturated source areas of surface run-off generation under the assumption of steady-state conditions and uniform soil properties. In the case of altitude, the highest weight (0.292) was for the range of 750–1009 m that has positive effect in flood occurrence. Finally, based on Equation (9), the final flood susceptibility map created by the SE model is shown in Figure 6.
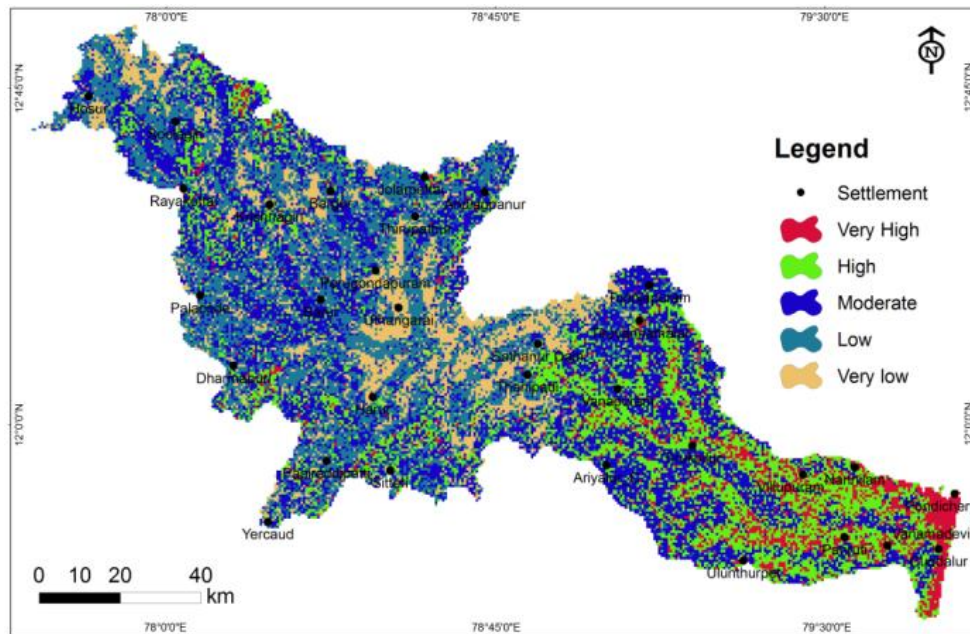
Figure 6: Flood susceptibility map of SE model in Ponnaiyar River basin

In flood susceptibility appraisal, the major aim was to find areas that may be affected by future floods. Thus, no matter which integration methodology is used, it is very important to validate the resultant flood susceptibility maps with respect to unknown future flood events (Chung & Fabbri, 2003). In this study, the flood locations that were not used during the model building/training were used to verify the flood susceptibility maps. The receiver operating characteristics (ROC) analysis was used (Egan, 1975; Swets, 1988; Pradhan & Lee, 2010; Pradhan et al., 2011; Pourghasemi et al., 2012a; Rahmati et al., 2014) to determine the accuracy of flood susceptibility maps produced using FR models. The ROC curve is a common methodology to determine the accuracy of a diagnostic test (Pourghasemi et al., 2012a), and it is considered as a graphical representation of the trade-off between the false-negative (X-axis) and false-positive (Y-axis) rates for every possible cut-off value (Pourghasemi et al., 2014). The AUC of ROC describes the accuracy of a prediction model by determining the system's ability to expect the correct occurrence or non-occurrence of pre-defined 'events' (Pourtaghi & Pourghasemi, 2015). The ROC curves for FR and SE models are shown in Figure 7 a & b respectively.
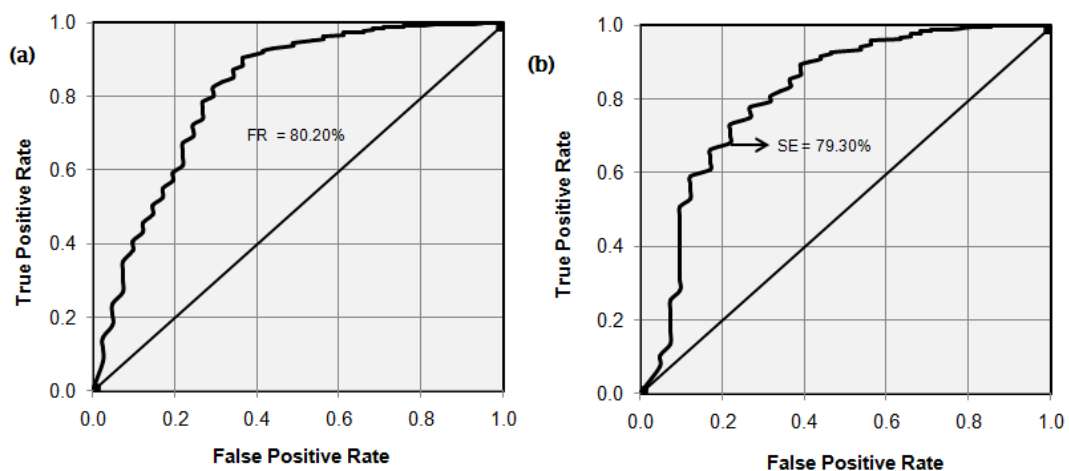

Figure 7: ROC curve for the flood susceptibility maps produced by FR and SE models of Ponnaiyar river basin

It is clear that in the flood susceptibility mapping using the FR model, the AUC is about 0.8020, which corresponds to the prediction accuracy of 80.20%, whereas in the flood susceptibility map using the SE model, the AUC is about 0.7930 and the prediction accuracy is 79.30%. Therefore, based on the calculated AUC, the FR and SE models indicated almost similar and reasonable results and can be used as simple tools in flood susceptibility mapping and flood mitigation when a sufficient number of data is obtained.

5. Conclusion

Industrial and agricultural expansion has been accompanied in recent decades by an ever increasing use of areas subject to flood, which has resulted in increased flood damages. Apart from studies related to investigations and improvements of river system, simultaneous action for studies of watersheds and adoption of measures aimded at runoff and water flow retardation is also required. Therefore, flood susceptibility mapping is necessary for integrated watershed management in order to have sustainable development. The validation of results indicated that the FR and SE models had almost similar and reasonable results in the study area. In the present study, flood susceptibility maps have been prepared using FR and SE methods with the integration of remote sensing and GIS. The application of the FR and SE models is divided into three steps: the construction of database, the calculation of weights and the data integration and verification procedure, in which the obtained FSI was verified with ROC and flood locations. In general, all used factors have relatively higher values of variation index implying the importance of all factors for accurate demarcation of flood prone areas. FR approach is in agreement with the result obtained by other researchers used in flood susceptibility appraisal and various environmental studies. FR model is effective and reliable approach for flood susceptibility mapping in the present study. According to Shannon's entropy results, it can be concluded that lithology and curvature have the strongest relationships with flood occurrence. Also, factors such as slope angle (degree) distance to from Main River, and slope aspect had the lowest importance on flood susceptibility map. From the analysis, it is seen that the FR model (AUC=80.20 %) performs better than SE (AUC=79.30 %) models. As a final conclusion, the results of the present study proved that FR and SE models can be successfully used in flood susceptibility mapping. So, the result of flood susceptibility map indicated that the Ponnaiyar river basin has undergone a significant amount of the flood occurrences are made in future. Based on the overall assessments, the proposed approaches in this study were concluded as objective and applicable. The scientific information derived from this study can assist governments, planners and engineers to perform proper actions in order to prevent and mitigate the flood occurrence in the future.

Acknowledgements

References

Aniya, M. Landslide-susceptibility mapping in the amahata river basin, Japan. *Ann Assoc Am Geogr.* 1985. 75 (1) 102-114.

Anbazhagan, S., and Dash, P. Environmental case study of Cauvery river flood plain. *GIS Development.* 2003. 7 (12) 30-35.

Ayazi, M.H., Pirasteh, S., Arvin, A.K.P., Pradhan, B., Nikouravan, B., and Mansor, S. Disasters and risk reduction in groundwater: Zagros mountain southwest Iran using geo-informatics techniques. *Dis Adv.* 2010. 3 (1) 51-57.

Bajabaa, S., Masoud, M., and Al-Amri, N. Flash flood hazard mapping based on quantitative hydrology, geomorphology and GIS techniques (case study of Wadi Al Lith, Saudi Arabia). *Arab. J. Geosci.* 2013. 1-13.

Bednarik, M., Magulová, B., Matys, M., and Marschalko, M. Landslide susceptibility assessment of the Kraľovany–Liptovský Mikuláš railway case study. *Phys Chem Earth*. 2010. 35; 162-171.

Charon, J.E., 1974: Hydrogeological applications of ERTS satellite imagery. In: Proc UN/FAO regional seminar on remote sensing of earth resources and environment. Commonwealth Science Council, Cairo. 439-456.

Chung, J.F., and Fabbri, A.G. Validation of spatial prediction models for landslide hazard mapping. *Nat Hazards.* 2003. 30 (3) 451-472.

Co, R.M., 1990: *Handbook of groundwater development.* New York: Wiley. 34-51.

Central Ground Water Board (CGWB), (2012). Annual Report.

Devkota, K.C., Regmi, A.D., Pourghasemi, H.R., Yoshida, K., Pradhan, B., Ryu, I.C., Dhital, M.R., and Althuwaynee, O.F. Landslide susceptibility mapping using certainty factor, index of entropy and logistic regression models in GIS and their comparison at Mugling–Narayanghat road section in Nepal Himalaya. *Nat Hazards.* 2013. 65; 135-165.

Egan, J.P., 1975: *Signal detection theory and ROC analysis*. New York: Academic Press.

Ercanoglu, M., and Gokceoglu, C. Assessment of landslide susceptibility for a landslide prone area (north of Yenice, NW Turkey) by fuzzy approach. *Environ Geol.* 2002. 41; 720-730.

Esteves, L.S. Consequences to flood management of using different probability distributions to estimate extreme rainfall. *J Environ Manage*. 2013. 115; 98-105.

Feng, C.C., and Wang, Y.C. GIScience research challenges for emergency management in southeast Asia. *Nat Hazards.* 2011. 59; 597-616.

Florinsky, I.V. Relationships between topographically expressed zones of flow accumulation and sites of fault intersection: analysis by means of digital terrain modelling. *Environ Model Softw.* 2000. 15 (1) 87-100.

Glenn C.R. et al., 2012: Lahaina Groundwater Tracer Study—Lahaina, Maui, Hawaii. Final Interim Report prepared from the State of Hawaii DOH, the U.S. EPA, and the U.S. Army Engineer Research and Development Center.

Geological Survey of India (GSI) (1988). Annual report.

Gokceoglu, C., and Aksoy, H. Landslide susceptibility mapping of the slopes in the residual soils of the Mengen region (Turkey) by deterministic stability analyses and image processing techniques. *Eng Geol.* 1966. 44; 147-161.

Jaafari, A., Najafi, A., Pourghasemi, H.R., Rezaeian, J., and Sattarian, A. GIS-based frequency ratio and index of entropy models for landslide susceptibility assessment in the Caspian forest, northern Iran. *Int J Environ Sci Te.* 2014. 11 (4) 909-926.

Joint Needs Assessment (JNA) Report of Tamilnadu Floods-2015.

Jourde, H., Lafare, A., Mazzilli, N., Belaud, G., Neppel, L., Dörfliger, N., and Cernesson, F. Flash flood mitigation as a positive consequence of anthropogenic forcing on the groundwater resource in a karst catchment. *Environ Earth Sci.* 2014. 71; 573-583.

Kia, M.B., Pirasteh, S., Pradhan, B., Mahmud, A.R., Sulaiman, W.N.A., and Moradi, A. An artificial neural network model for flood simulation using GIS: Johor river basin, Malaysia. *Environ Earth Sci.* 2012. 67; 251-264.

Kjeldsen, T.R. Modelling the impact of urbanization on flood frequency relationships in the UK. *Hydrol. Res.* 2010. 41; 391-405.

Lee, S., Kim, Y.S., and Oh, H.J. Application of a weights-of-evidence method and GIS to regional groundwater productivity potential mapping. *Environ Manag.* 2012a. 96 (1) 91-105.

Liu, Y.B., Gebremeskel, S., De Smedt F. et al. A diffusive transport approach for flow routing in GIS-based flood modeling. *J Hydrol.* 2003. 283; 91-106.

Masood, M., and Takeuchi, K., Assessment of flood hazard, vulnerability and risk of mid-eastern Dhaka using DEM and 1D hydrodynamic model. *Nat Hazards.* 2012. 61; 757-770.

Massey, D.S., and Nancy, A.D. The Dimensions of Residential. *Social Forces.* 1988. 67 (2) 281-315.

Mogaji, K.A., Lim, H.S., and Abdullah, K. Regional prediction of groundwater potential mapping in a multifaceted geology terrain using GIS-based Dempster–Shafer model. *Arab J Geosci.* 2015. 8 (5) 3235-3258.

Moore, I.D., Grayson, R.B., and Ladson, A.R. Digital terrain modeling: a review of hydrological, geomorphological and biological applications. *Hydrol Process.* 1991. 5; 3-30.

Pourghasemi, H.R., and Beheshtirad, M. Assessment of a data-driven evidential belief function model and GIS for groundwater potential mapping in the Koohrang Watershed, Iran. *Geocarto Int.* 2014. 30 (6) 662-685.

Pourghasemi, H.R., Mohammady, M., and Pradhan, B. Landslide susceptibility mapping using index of entropy and conditional probability models in GIS: Safarood Basin, Iran. *Catena.* 2012a. 97; 71-84.

Pradhan, B., and Lee, S. Regional landslide susceptibility analysis using back-propagation neural network model at Cameron Highland, Malaysia. *Landslides.* 2010. 7 (1) 13-30.

Pradhan, B. Flood Susceptible Mapping and Risk Area Estimation Using Logistic Regression, GIS and Remote Sensing. *J Spatial Hydrol.* 2012a. 9 (2) 1-18.

Pradhan, B. Remote sensing and GIS-based landslide hazard analysis and cross-validation using multivariate logistic regression model on three test areas in Malaysia. *Adv Space Res.* 2010b. 45 (10) 1244-1256.

Pradhan, B., and Buchroithner, M.F. Comparison and validation of landslide susceptibility maps using an artificial neural network model for three test areas in Malaysia. *Environ. Eng. Geosci.* 2010. 16; 107-126.

Pradhan, B., Youssef, A.M., and Varathrajoo, R. Approaches for delineating landslide hazard areas using different training sites in an advanced artificial neural network model. *Geospatial. Inf. Sci.* 2010b. 13; 93-102.

Pradhan, B., Mansor, S., Pirasteh, S., and Buchroithner, M.F. Landslide hazard and risk analyses at a landslide prone catchment area using statistical based geospatial model. *Int. J. Remote. Sens.* 2011. 32; 4075-4087.

Pradhan, B. Use of GIS-based fuzzy logic relations and its cross application to produce landslide susceptibility maps in three test areas in Malaysia. *Environ. Earth Sci.* 2011. 63; 329-349.

Pourtaghi, Z.S., and Pourghasemi, H.R. GIS-based groundwater spring potential assessment and mapping in the Birjand Township, southern Khorasan Province, Iran. *Hydrogeol J.* 2015. 22; 643-662.

Rahmati, O., Pourghasemi H.R. and Zeinivand, H. Flood susceptibility mapping using frequency ratio and weights-of-evidence models in the Golastan Province, Iran. *Geocarto International*, 2015. 31 (1) 42-70.

Rahmati, O., Nazari Samani, A., Mahdavi, M., Pourghasemi, H.R., and Zeiniv, H. Groundwater potential mapping at Kurdistan region of Iran using analytic hierarchy process and GIS. *Arab J Geosci.* 2014a. 8; 1-13.

Regmi, A.D., Devkota, K.C., Yoshida, K., Pradhan, B., Pourghasemi, H.R., Kumamoto, T., and Akgun, A. Application of frequency ratio, statistical index, and weights-of-evidence models and their comparison in landslide susceptibility mapping in central Nepal Himalaya. *Arab J Geosci.* 2013.

Saha, A.K., Gupta, R.P., Sarkar, I., Arora, K.M., and Csaplovics, E. An approach for GIS-based statistical landslide susceptibility zonation with a case study in the Himalayas. *Landslides.* 2005. 2; 61-69.

Schober, B., Hauer, C., and Habersack, H. A novel assessment of the role of Danube floodplains in flood hazard reduction (FEM method). *Nat Hazards.* 2015. 75; 33-50.

Shafapour Tehrany, M., Pradhan, B., and Jebur, M.N. Spatial prediction of flood susceptible areas using rule based decision tree (DT) and a novel ensemble bivariate and multivariate statistical models in GIS. *J Hydrol.* 2013. 504; 69-79.

Smith, K., and Ward, R., 1998: *Floods: Physical Processes and Human Impacts.* Chichester: Wiley. 382.

Swets, J.A. Measuring the accuracy of diagnostic systems. *Science.* 1988. 240; 1285-1293.

Tehrany, M.S., Pradhan, B., Jebur, M.N. Spatial prediction of flood susceptible areas using rule based decision tree (DT) and a novel ensemble bivariate and multivariate statistical models in GIS. *J Hydrol.* 2013. 504; 69-79.

Tehrany, M.S., Pradhan, B., Jebur, M.N. Flood susceptibility mapping using a novel ensemble weights-of-evidence and support vector machine models in GIS. *J Hydrol.* 2014. 512; 332-343.

Theil, H., 1972: *Statistical decomposition analysis.* Amsterdam: North-Holland Publishing Company.

Vieux, B.E., 2004: *Distributed hydrologic modeling using GIS.* Water Sci Tech Libr. Vol. 48. Kluwer Academic Publishers. 312.

Wang, H.B., Wu, S.R., Shi, J.S., and Li, B. Qualitative hazard and risk assessment of landslides: a practical framework for a case study in China. *Nat Hazards.* 2013. 69; 1281-1294.

Yalcin, A. GIS-based landslide susceptibility mapping using analytical hierarchy process and bivariate statistics in Ardesen (Turkey): comparisons of results and confirmations. *Catena.* 2008. 72. 1-12.

Yufeng, S., and Fengxiang, J. Landslide stability analysis based on generalized information entropy. *Int Conf Environ Sci Inf Appl Technol.* 2009. 2; 83-85.